Acta Crystallographica Section D
Biological Crystallography
ISSN 0907-4449

Structures of aminoglycoside acetyltransferase AAC(6′)-Ii in a novel crystal form: structural and normal-mode analyses

David L. Burk,[a] Bing Xiong,[a] Caroline Breitbach[b] and Albert M. Berghuis[a,b]*

[a]Department of Biochemistry, McGill University, 740 Dr Penfield Avenue, Montreal, QC, H3A 1A4, Canada, and [b]Departments of Microbiology and Immunology, McGill University, 3775 University Street, Montreal, QC, H3A 2B4, Canada

Correspondence e-mail: albert.berghuis@mcgill.ca

Received 3 May 2005
Accepted 5 July 2005

PDB Reference: AAC(6′)-Ii, 2a4n, r2a4nsf.

The aminoglycoside-modifying enzyme aminoglycoside 6′-*N*-acetyltransferase type Ii [AAC(6′)-Ii] has been crystallized with its cofactor coenzyme A in space group $C222_1$, with unit-cell parameters a = 71.5, b = 127.4, c = 76.9 Å and one physiologically relevant dimer species per asymmetric unit. The space group previously observed for this complex was $P2_12_12_1$, with two dimers per asymmetric unit. By comparing the six available protomer structures of the AAC(6′)-Ii–CoA complex, it has been possible to identify regions of plasticity within the protein. Normal-mode analysis of this complex suggests that this plasticity is not an artefact of crystal-packing forces, but that the region of the protomer that displays multiple conformations is intrinsically flexible. It is conjectured that the flexibility is relevant for the cooperative activity observed for the enzyme.

1. Introduction

The aminoglycosides are a family of structurally diverse antibiotics that are effective against a broad spectrum of clinically important pathogenic organisms. Aminoglycosides are believed to exert their bactericidal effects by binding to the 16S rRNA of the 30S ribosomal fragment, where they interfere with the fidelity of protein synthesis and lead to the formation of misfolded proteins (Woodcock *et al.*, 1991; Moazed & Noller, 1987; Fourmy *et al.*, 1996; Davis, 1987; Davis *et al.*, 1986). In addition to their effects on translation, aminoglycosides are also observed to disrupt the bacterial outer membrane and interfere with the initiation of DNA replication (Matsunaga *et al.*, 1986). Despite their potential for nephrotoxicity and ototoxicity, aminoglycosides have remained therapeutically valuable owing to their desirable concentration-dependent bactericidal action, relatively well understood pharmacokinetics and synergism with other antibiotics. However, the therapeutic use of these compounds is being compromised by the appearance of organisms resistant to their effects. Although not the only mechanism of resistance, enzymatic modification by bacterial aminoglycoside-modifying enzymes is the most clinically relevant. There are three general classes of these enzymes: aminoglycoside *N*-acetyltransferases, *O*-adenyltransferases and *O*-phosphotransferases. All three groups of enzymes act by decreasing the affinity of the aminoglycoside for the bacterial ribosome, abolishing their antibiotic activity (Llano-Sotelo *et al.*, 2002). N-Acetylation at the 6′ position is one of the more common types of aminoglycoside modification (Miller *et al.*, 1997). In *Enterococcus faecium*, the chromosomally encoded enzyme AAC(6′)-Ii confers low-level aminoglycoside resistance by catalyzing this reaction (Costa *et al.*, 1993). AAC(6′)-Ii was

first characterized by Wright and Ladak, who showed the enzyme to be a homodimer in solution with broad substrate specificity for both 4,5- and 4,6-disubstituted deoxystreptamine aminoglycosides (Wright & Ladak, 1997). More recently, it has been shown that AAC(6′)-Ii follows an ordered bi–bi ternary complex mechanism and that there is evidence of cooperativity between the two protomers (Draker *et al.*, 2003).

The determination of the crystal structure of the AAC(6′)-Ii–acetyl-CoA complex identified the enzyme as a member of the GCN5-related *N*-acetyltransferase (GNAT) superfamily of enzymes (Wybenga-Groot *et al.*, 1999). The crystal structures of a number of other GNAT superfamily enzymes are now available, revealing remarkable structural homologies in a group of enzymes with diverse substrates (Bhatnagar *et al.*, 1998; Dutnall *et al.*, 1998; Hickman *et al.*, 1999; Peneff *et al.*, 2001). More recently, the physiological dimer of AAC(6′)-Ii has been unambiguously identified and the oligomeric arrangement has been compared with those of other GNAT-superfamily members (Burk *et al.*, 2003). Our understanding of the molecular mechanism of the GNAT-superfamily enzymes remains incomplete, despite the availability of structural and kinetic data. In order to gain insight into the mechanism of AAC(6′)-Ii, we are pursuing structures of the enzyme in complex with a series of enzyme inhibitors. As part of these efforts, we have solved the structure of an AAC(6′)-Ii–CoA complex in a space group not previously observed for this molecule. Analysis of this new crystal form, combined with a normal-mode analysis of AAC(6′)-Ii, allowed us to identify conformational changes that may be involved in the mechanism of this enzyme.

2. Materials and methods

2.1. Crystallization and data collection

AAC(6′)-Ii was overexpressed in *Escherichia coli* BL21(DE3) cells and purified to homogeneity according to a previously published protocol (Wright & Ladak, 1997). Purified protein was concentrated to ∼7 mg ml^{-1} using Vivaspin 20 (Vivascience AG) concentrators and stored at 277 K. This purified protein was used to set up co-crystallization trials that included AAC(6′)-Ii, coenzyme A and the inhibitor 2-(6′-*N*-sisomycin)acetic acid.

Screening of crystallization conditions was performed using the hanging-drop vapour-diffusion technique at 277 and 295 K. A promising crystallization condition was identified using the Crystal Screen 2 kit from Hampton Research (Aliso Viejo, CA, USA). Optimization of this condition resulted in diffraction-quality crystals that grew to dimensions of 0.3 × 0.2 × 0.1 mm in approximately six weeks. The crystals used for data collection were obtained from a 4 µl drop consisting of 2 µl protein solution [25 m*M* HEPES pH 7.5, 2 m*M* EDTA, a twofold molar excess of coenzyme A and a twofold molar excess of 2-(6′-*N*-sisomycin)acetic acid] and an equal volume of reservoir solution (0.1 *M* trisodium citrate pH 5.6, 2.1 *M* ammonium sulfate). The reservoir contained a total of 0.6 ml precipitant solution and was covered with 0.4 ml of a 2:1 silicone:paraffin oil mixture.

For data collection, crystals were briefly transferred to mother liquor saturated with sucrose and then flash-frozen by plunging them into liquid nitrogen. Diffraction data to 2.2 Å resolution were collected at the X8C beamline of the National Synchrotron Light Source (Brookhaven National Laboratoy, Upton, NY, USA) using an ADSC Quantum 4 CCD detector (λ = 1.072 Å).

Table 1
Data-collection and refinement statistics.

Resolution (Å)	2.2
Unit-cell parameters (Å, °)	a = 71.48, b = 127.35, c = 76.91, $\alpha = \beta = \gamma$ = 90
No. of observations	117103
No. of unique reflections	18161
$\langle I\rangle/\langle\sigma(I)\rangle$†	19.2 (5.5)
$R_{\rm merge}$‡	0.076 (0.233)
Completeness (%)	99.0 (91.2)
$R_{\rm cryst}$§	0.199 (0.217)
$R_{\rm free}$	0.252 (0.294)
No. of protein atoms	2884
No. of solvent molecules	198
No. of ions	2
Estimated overall thermal factor (Wilson plot) (Å^2)	34.2
Mean thermal factor (Å^2)	
Main-chain atoms	26.4
Side-chain atoms	27.9
R.m.s. deviation from ideal geometry	
Bond lengths (Å)	0.006
Bond angles (°)	1.3°
Estimated overall coordinate error (Å)	
$\sigma_{\rm A}$ (Read, 1986)	0.16
DPI (Cruickshank, 1999)	0.38

† $\langle I\rangle$ is the mean intensity for all reflections and $\langle\sigma(I)\rangle$ is the mean σ for these reflections. ‡ $R_{\rm merge} = \sum\sum|I_i - \langle I\rangle|/\sum\sum\langle I\rangle$, where I_i is the intensity of an individual measurement of a reflection and $\langle I\rangle$ is the mean value for all equivalent measurements of this reflection. § $R_{\rm cryst} = \sum||F_{\rm o}| - |F_{\rm c}||/\sum|F_{\rm o}|$.

2.2. Data processing and structure refinement

The programs *DENZO* and *SCALEPACK* were used to integrate and scale the diffraction data (Otwinowski & Minor, 1997). The crystals were found to belong to the orthorhombic space group $C222_1$, a space group not previously observed with this protein. Unit-cell parameters and statistics associated with data processing are shown in Table 1.

The structure was solved by molecular replacement using the *CNS* suite of programs (Brünger *et al.*, 1998). The search model consisted of an AAC(6′)-Ii dimer constructed from the coordinates of the AAC(6′)-Ii–CoA complex (PDB code 1n71) from which solvent and cofactor atoms had been removed. One AAC dimer per asymmetric unit gave a calculated Matthews coefficient of 2.11 Å^3 Da^{-1}, which is in the range expected for a protein crystal and suggests a solvent content of approximately 50%. A fast direct rotation search using 10–4 Å data yielded two orientations (7σ and 6.6σ) that were significantly better than the other solutions (all <3σ). The solutions reflect the presence of near-perfect twofold symmetry relating the two protomers in the dimer search

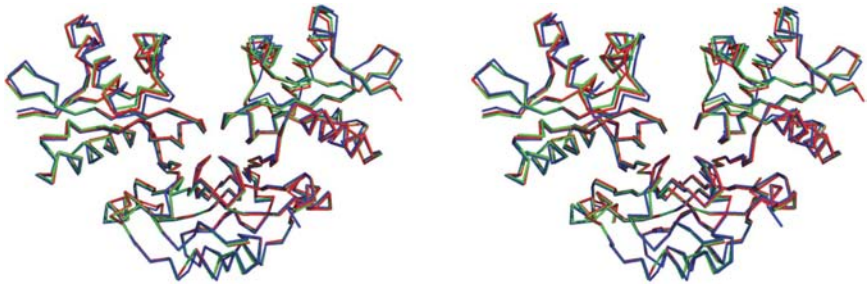

Figure 1
A stereo figure showing the superimposed C^{α} backbones of AAC(6′)-Ii in the $P2_12_12_1$ (blue and green) and $C222_1$ (magenta) crystal forms.

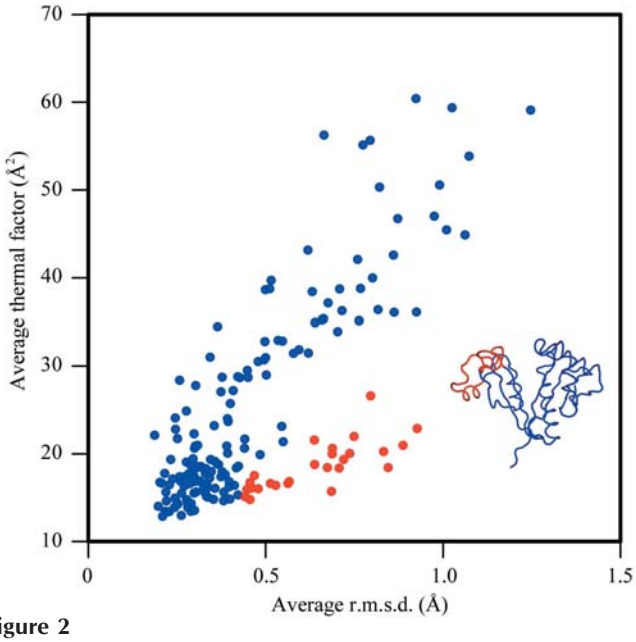

Figure 2
A plot of average thermal factor *versus* average r.m.s. deviation in main-chain atomic coordinates for all available structures of AAC(6′)-Ii–CoA. Each symbol corresponds to one residue in the AAC(6′)-Ii structure. The residues have been placed into two groups based on visual inspection of the plot and coloured red and blue. Those residues exhibiting the expected relationship between average thermal factor and average r.m.s. deviation are coloured blue. Those residues with unusually low thermal factors are shown in red. The inset shows a C^{α} backbone trace of AAC(6′)-Ii illustrating the location of the two groups of residues.

model. A translation search was then performed using a general translation function (fastf2f2 target, 10–4 Å data), with the top solution from the rotation search yielding the best translation-search solution. This model was then subjected to two cycles of alternating positional and thermal factor refinement using a maximum-likelihood target function and data to 2.2 Å resolution. Examination of $2F_o - F_c$ and $F_o - F_c$ maps revealed unambiguous electron density consistent with a coenzyme A molecule in the active sites of both protein molecules and these were added to the model at this time. Alternating cycles of refinement (positional and thermal factor) and manual adjustment were continued, with sulfate ions and water molecules incorporated into the model in the latter stages of refinement. Refinement was discontinued when no further improvement in R_{free} was observed. At no time during the course of model refinement was evidence of the 2-(6′-*N*-sisomycin)-acetic acid inhibitor observed in either active site.

2.3. Normal-mode analysis

Normal-mode analysis was performed using standard techniques as implemented in the *VIBRAN* module of the *CHARMM* program and using the CHARMM22 empirical energy function for all atoms (Brooks *et al.*, 1983; MacKerell *et al.*, 1998). To account for the shielding of distant charges by solvent, a distance-dependent dielectric constant was used and the atomic charges on ionic side chains were scaled by a factor of 0.3. Energy minimization of the AAC(6′)-Ii structure was carried out *via* 500 cycles of steepest descent minimization, followed by the Adapted Basis Newton–Raphson method. The minimizations were terminated when the r.m.s. energy gradient reached 4×10^{-8} kJ mol^{-1} Å^{-1}. Calculations were carried out on the dimer form of AAC(6′)-Ii with bound coenzyme A so as to obtain physiologically relevant insights into the complex for which the crystal structures were determined. In our analyses, only the lowest frequency modes were considered because these modes give rise to large displacements and provide information on the important intradomain and interdomain motions.

3. Results and discussion

The initial aim of this study was to determine the structure of AAC(6′)-Ii in complex with coenzyme A and the inhibitor 2-(6′-*N*-sisomycin)acetic acid. Our preliminary results were encouraging, with the protein crystallizing in a space group different to that observed for the structure of AAC(6′)-Ii in complex with coenzyme A alone. However, at no time during refinement could evidence be found in electron-density maps for the presence of 2-(6′-*N*-sisomycin)acetic acid. Symmetry-related molecules were found to be positioned near the active-site clefts of the two enzyme molecules and it is possible that this interferes with binding of the inhibitor. Therefore, the structure is that of the AAC(6′)-Ii–CoA complex in a new crystal form.

Despite crystallizing in different space groups, the dimer arrangements of the AAC(6′)-Ii–CoA complexes are essentially identical (Fig. 1). There are differences in the positions in some of the secondary-structural elements between the AAC(6′)-Ii protomers in the two crystal forms. By examining the differences between the different structures of AAC(6′)-Ii–CoA, we may to be able to identify regions of structural variability in this enzyme that could shed light on molecular motions important to its mechanism.

3.1. AAC(6′)-Ii–CoA structure I: variations *versus* flexibility

The first crystal form of the AAC(6′)-Ii–CoA complex crystallized in space group $P2_12_12_1$, with four protomers in the

asymmetric unit (hereafter referred to as P_I, P_{II}, P_{III} and P_{IV}). These molecules, combined with the two from the asymmetric unit of the $C222_1$ crystal form described here (hereafter referred to as C_I and C_{II}), make a total of six crystallographically independent structures of the AAC(6′)-Ii–CoA complex available for analysis. (Note: non-crystallographic symmetry restraints and constraints were not employed during refinement for either crystal form.) One method that can identify potentially interesting regions of a protein molecule is the analysis of root-mean-square difference (r.m.s.d.) in atomic coordinates and crystallographic thermal factor.

When comparing the atomic coordinates of superimposed protein structures, regions with large r.m.s.d. values can arise from two very different situations. The observed differences in atomic positions may be the result of conformational differences in the molecules in these areas. In other cases, the observed differences are illusory, in that they arise from differential fitting of the protein model in regions of poor-quality electron density. These situations can perhaps be differentiated by examining the thermal factors of the residues in question. In the former case, in which there are significant conformational changes, the thermal factors will have values inconsistent with poor density. In the case of differential fitting to poor density, the average thermal factors will be comparatively higher.

The average r.m.s.d. in main-chain atomic coordinates between the six AAC(6′)-Ii molecules ranges from 0.15 to 0.79 Å. Fig. 2 depicts the average r.m.s.d. of the atomic positions of the main-chain atoms *versus* their average thermal factor. Most of the residues in the AAC(6′)-Ii structures (blue symbols) belong to the second group mentioned in the previous paragraph: that is, residues whose increasing thermal factors are explained by differential fitting to poor electron density. Residues with increasing average r.m.s.d. values are seen to also possess increasing average thermal factors, producing a roughly linear distribution. A number of the residues, however, show relatively high r.m.s.d. values coupled with unusually low thermal factors (red symbols). This suggests that these sections of the polypeptide backbone exist in a small number of significantly different relatively non-flexible conformations. This may reflect a biologically relevant conformational change or, alternatively, differences in protein conformation resulting from different crystal-packing interactions.

Using Fig. 2 as a guide, residues with relatively low thermal factors coupled with higher than expected r.m.s. differences in coordinates were inspected using computer graphics. As can be seen in the inset of Fig. 2, these residues (residues 113–136 and 160–166) form the outer face of the C-terminal lobe of AAC(6′)-Ii.

3.2. AAC(6′)-Ii–CoA structure II: lobe movement

An alternative method for analyzing the structures of the AAC(6′)-Ii–CoA crystal forms is to calculate difference distance matrices. This method allows the comparison of two structures without the bias that would be introduced by least-squares superposition of the structures. Matrices were calculated to compare the four molecules in the $P2_12_12_1$ asymmetric unit and the two molecules in the $C222_1$ asymmetric unit (Fig. 3). This procedure identified residues 105–165 as the section of the AAC(6′)-Ii molecule with the most significant deviations in backbone coordinates. This region corresponds to the majority of the C-terminal lobe of AAC(6′)-Ii.

The AAC(6′)-Ii structures can be organized into three groups of similar structure based on features in the difference distance matrices. The lack

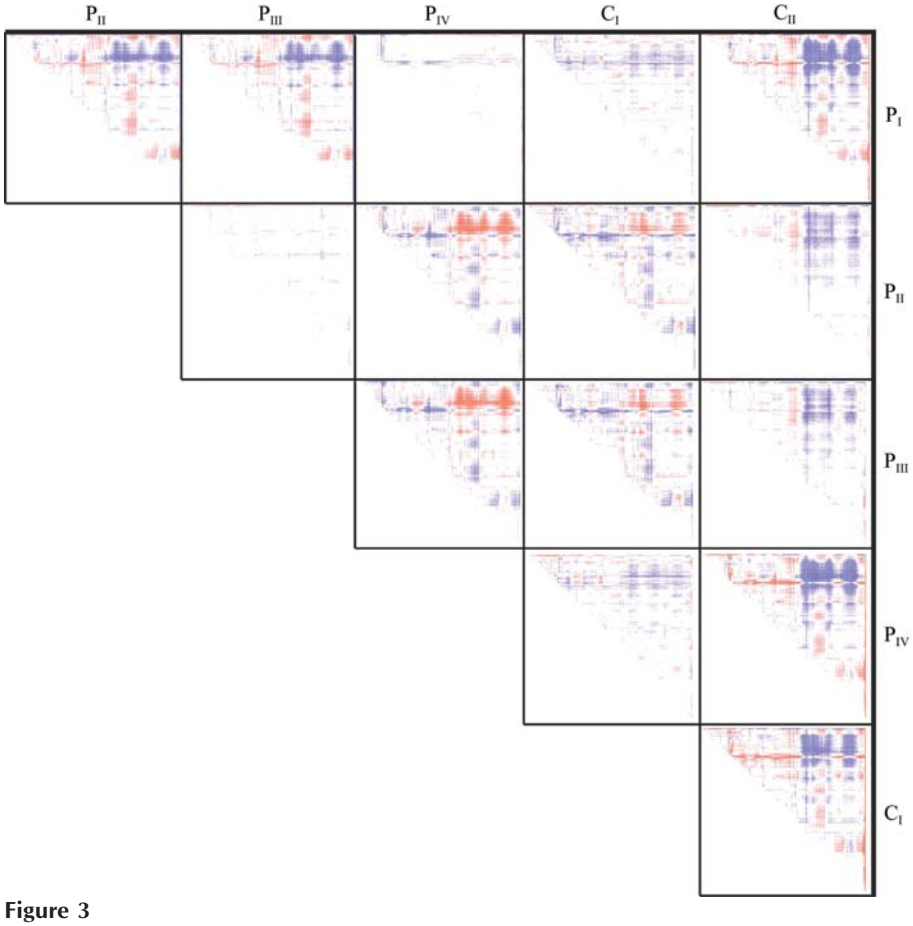

Figure 3
Difference distance matrix comparing the structures of the four protomers from the $P2_12_12_1$ crystal form (P_I, P_{II}, P_{III} and P_{IV}) and the two protomers from the $C222_1$ crystal form (C_I and C_{II}) of AAC(6′)-Ii–CoA. The difference values are plotted with colours, with the darkest red representing a value of −1.5 Å, white representing 0 Å and the darkest blue 1.5 Å. Difference distance matrix plots were produced using the *DDMP* program from the Center for Structural Biology at Yale University, New Haven, CT, USA.

of features in two boxes of the top row of the matrix indicates that the P_I, C_I and P_{IV} molecules form one such group. Similarly, the second row of the matrix shows that the P_{II} and P_{III} molecules have essentially the same conformation. The remaining molecule, C_{II}, forms a third group as it is not similar to any of the others.

Representative structures from each of the three groups (P_I, P_{II} and C_{II}) were superimposed using a least-squares methods. From Fig. 3, it is apparent that the N-terminal lobes of the AAC(6′)-Ii structures are very similar, except for a short section between approximately residues 28–35. By using the coordinates of the N-terminal lobe (except residues 28–35) in the least-squares calculation, significant positional differences in the C-terminal lobe are revealed (Fig. 4*a*). Most notable are positional differences for residues 114–140 and 158–168. These residues form the outer part of the C-terminal lobe of AAC(6′)-Ii. The two lobes of the AAC(6′)-Ii molecule are arranged in a V-shape, with the coenzyme A cofactor binding

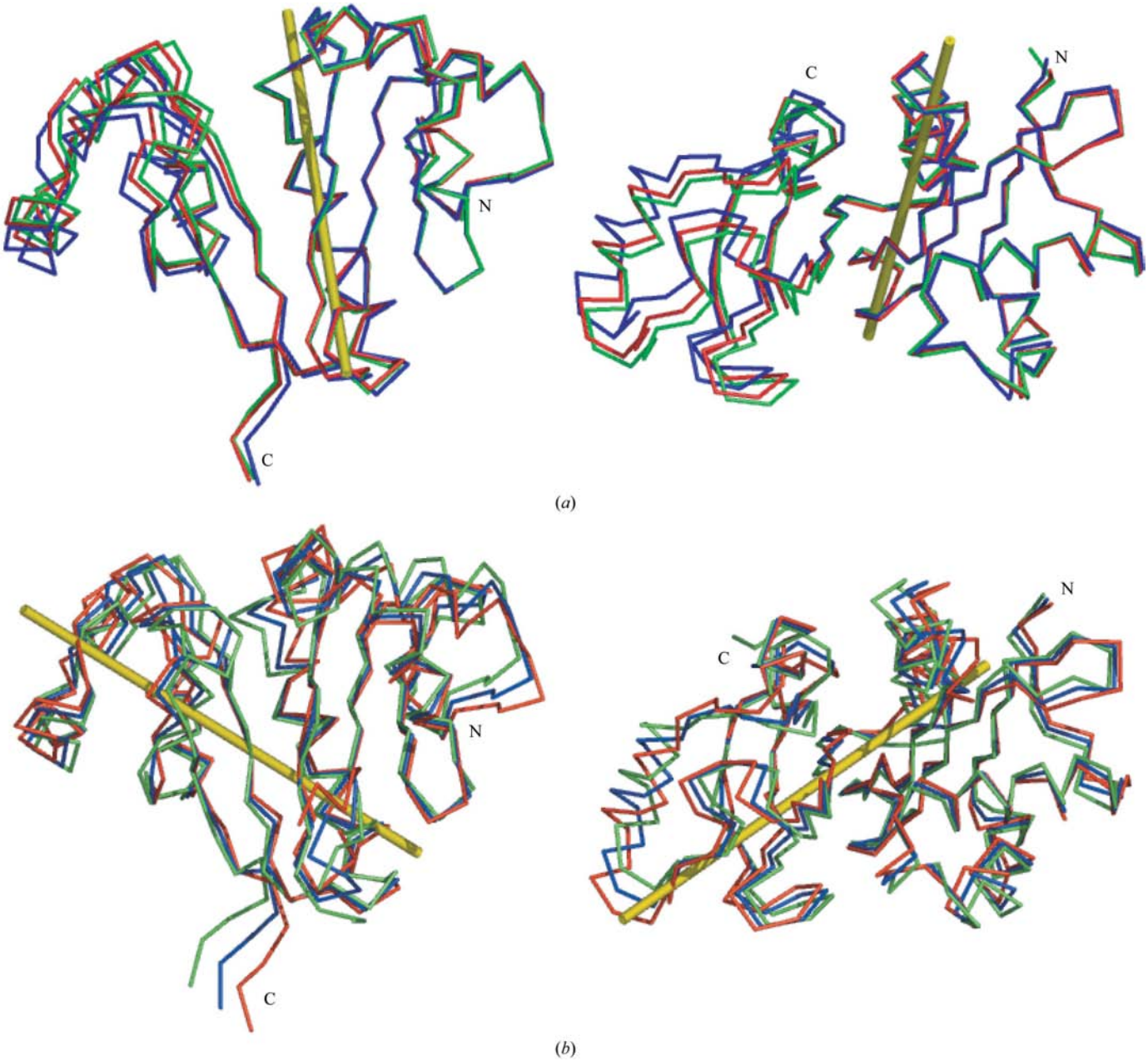

Figure 4
(*a*) A superposition (using the coordinates of the N-terminal lobe) of representatives of the three groups of AAC(6′)-Ii structures revealed by the difference distance analysis. The axis describing the relationship between the structures is shown as a yellow rod. The position of the rotation axis was determined using the program *DYNDOM* (Hayward & Berendsen, 1998). The right panel is a 90° rotation of the left panel about a horizontal axis through the centre of the molecule, providing a 'top-down' view of the molecules. (*b*) An illustration of the motion related to the lowest frequency normal mode of AAC(6′)-Ii. The crystal structure of AAC(6′)-Ii following energy minimization is shown in blue. The structures coloured red and green were generated from the lowest frequency normal mode and reflect the motion of the structure about the minimized crystal structure. The axis about which the motion occurs, calculated as described above, is shown by a yellow rod.

in the cleft between the arms of the V. The structures examined here represent varying degrees of 'openness' of the cleft between the lobes. The amplitude of this change is significant, with a rotation of approximately 8° about the axis shown. The change in position of the C-terminal lobe appears to originate with a small change in the φ angles of residue 108 (∼10°) and compensatory change in the φ angle of residue 170 (∼5°).

3.3. Comparison of observed plasticity and normal-mode analysis

Both structural comparison methods identify the C-terminal lobe of AAC(6)-Ii as a region of significant plasticity, with the difference distance matrix analysis suggesting that the plasticity is related to various degrees of openness of the cleft between the two lobes. However, as mentioned before, the observed plasticity may be an artefact induced by crystal packing and may not reflect the natural movements in the enzyme. Examination of crystal-packing interactions for the different protomers in the two crystal forms reveals that residues of the C-terminal lobe are involved in crystal-packing interactions. Hence, this is a viable explanation. To address this, we performed normal-mode analysis on the physiological dimer species in complex with CoA, the results of which are depicted in Fig. 4(*b*).

As can be seen in Fig. 4(*b*), normal-mode analysis also suggests that the C-terminal lobe is particularly flexible, in agreement with the crystallographic analysis. Specifically, residues 112–143 and 154–171 are implicated. Therefore, the various conformations of the AAC(6′)-Ii C-terminal lobe in the two different crystal forms most likely reflect the inherent plasticity of this portion of the enzyme structure. However, there is not perfect agreement between the crystallographic data and the normal-mode analysis. The rotation axis identified by either method is different. While the crystallographic analysis suggests that the cleft is the fulcrum (parallel to helix α3), the normal-mode analysis has the axis of rotation parallel to the C-terminal β-sheet.

3.4. Plasticity and enzymatic mechanism

As elegantly articulated by Koshland, conformational flexibility is an essential aspect of enzyme activity (Koshland & Neet, 1968). For AAC(6)-Ii conformational (flexibility) differences have experimentally been detected. Specifically, both NMR and proteolysis experiments reveal that the enzyme is more closed and compact when cofactor and substrate are bound (Draker and Wright, personal communications). This mirrors observations for the structurally related yeast histone acetyl transferase yHat1, which is also less susceptible to proteolysis when complexed with coenzyme A, suggesting that a conformational change occurs upon cofactor binding (Dutnall *et al.*, 1998). The data presented here do not address conformational changes upon substrate and/or cofactor binding, as they only deal with the CoA-bound state of the enzyme. However, the data may provide insight into the structural basis for cooperativity observed for AAC(6′)-Ii.

Wright and coworkers have noted that the two cofactor- and substrate-binding sites present in the physiological dimer species are not equivalent, in that binding of ligand to one protomer affects binding to the other protomer (Draker *et al.*, 2003). This observation suggests some form of communication between the two protomers. However, at least for the cofactor, the binding sites are sufficiently separated to exclude direct interference (Burk *et al.*, 2003). The plasticity analysis data presented here suggest that communication on the occupation state of cofactor (and perhaps also substrate) binding sites may occur through the C-terminal lobe. Particularly notable are residues 128–135 (helix α4), a region noted for its plasticity by both structural and normal-mode analyses and one which is intimately involved in the dimer interface (Burk *et al.*, 2003). In the dimer helix α4 forms interactions with the identical helix of the second protomer. These interactions are predominantly hydrophobic in nature, involving the benzyl moiety of Phe130, but also including hydrogen bonds between Thr129 and Lys153. In this scenario, binding of cofactor and/or substrate to one protomer affects the conformation/flexibility of the protomer, as suggested by NMR and proteolysis studies; this change in dynamic properties is used as the signal, communicated through helix α4, to inform the other protomer of a change in occupation state. Changes in helix α4 are most likely to alter the conformational flexibility of the second protomer, subtly affecting binding affinities for cofactor and substrate. Note that helix α4 is not a conserved structural element within the GNAT superfamily (Wybenga-Groot *et al.*, 1999). Furthermore, the oligomeric arrangement observed in AAC(6′)-Ii is also unique within dimeric GNAT-superfamily members (Burk *et al.*, 2003). Therefore, it is questionable that the proposed structural basis for protomer cooperativity can be extended beyond AAC(6′)-Ii.

This work was supported by a grant from the Canadian Institutes of Health Research. CJB acknowledges support from an NSERC Undergraduate Student Research Award. AMB is the recipient of the Canada Research Chair in Structural Biology. Support for beamline X8C at the NSLS-BNL, Upton, New York was received in part from the Natural Sciences and Engineering Council of Canada and the Canadian Institutes of Health Research.

References

Bhatnagar, R. S., Futterer, K., Farazi, T. A., Korolev, S., Murray, C. L., Jackson-Machelski, E., Gokel, G. W., Gordon, J. I. & Waksman, G. (1998). *Nature Struct. Biol.* **5**, 1091–1097.

Brooks, B. R., Bruccoleri, R. E., Olafson, B. D., States, D. J., Swaminathan, S. & Karplus, M. (1983). *J. Comput. Chem.* **4**, 187–217.

Brünger, A. T., Adams, P. D., Clore, G. M., DeLano, W. L., Gros, P., Grosse-Kunstleve, R. W., Jiang, J.-S., Kuszewski, J., Nilges, M., Pannu, N. S., Read, R. J., Rice, L. M., Simonson, T. & Warren, G. L. (1998). *Acta Cryst.* D**54**, 905–921.

Burk, D. L., Ghuman, N., Wybenga-Groot, L. E. & Berghuis, A. M. (2003). *Protein Sci.* **12**, 426–437.

Costa, Y., Galimand, M., Leclercq, R., Duval, J. & Courvalin, P. (1993). *Antimicrob. Agents Chemother.* **37**, 1896–1903.

Cruickshank, D. W. J. (1999). *Acta Cryst.* D**55**, 583–601.
Davis, B. D. (1987). *Microbiol. Rev.* **51**, 341–350.
Davis, B. D., Chen, L. L. & Tai, P. C. (1986). *Proc. Natl Acad. Sci. USA*, **83**, 6164–6168.
Draker, K. A., Northrop, D. B. & Wright, G. D. (2003). *Biochemistry*, **42**, 6565–6574.
Dutnall, R. N., Tafrov, S. T., Sternglanz, R. & Ramakrishnan, V. (1998). *Cell*, **94**, 427–438.
Fourmy, D., Recht, M. I., Blanchard, S. C. & Puglisi, J. D. (1996). *Science*, **274**, 1367–1371.
Hayward, S. & Berendsen, H. J. (1998). *Proteins*, **30**, 144–154.
Hickman, A. B., Klein, D. C. & Dyda, F. (1999). *Mol. Cell*, **3**, 23–32.
Koshland, D. E. Jr & Neet, K. E. (1968). *Annu. Rev. Biochem.* **37**, 359–410.
Llano-Sotelo, B., Azucena, E. F. Jr, Kotra, L. P., Mobashery, S. & Chow, C. S. (2002). *Chem. Biol.* **9**, 455–463.
MacKerell, A. D. Jr, Brooks, B., Brooks, C. L. III, Nilsson, L., Roux, B., Won, Y. & Karplus, M. (1998). *Encyclopedia of Computational Chemistry*, edited by P. v. R. Schleyer, N. L. Allinger, T. Clark, J. Gasteiger, P. A. Kollman, H. F. Schaefer III & P. R. Schreinere, pp. 271–277. Chichester: John Wiley & Sons.
Matsunaga, K., Yamaki, H., Nishimura, T. & Tanaka, N. (1986). *Antimicrob. Agents Chemother.* **30**, 468–474.
Miller, G. H., Sabatelli, F. J., Hare, R. S., Glupczynski, Y., Mackey, P., Shlaes, D., Shimizu, K. & Shaw, K. J. (1997). *Clin. Infect. Dis.* **24**, *Suppl.* 1, S46–S62.
Moazed, D. & Noller, H. F. (1987). *Nature (London)*, **327**, 389–394.
Otwinowski, Z. & Minor, W. (1997). *Methods Enzymol.* **276**, 307–326.
Peneff, C., Mengin-Lecreulx, D. & Bourne, Y. (2001). *J. Biol. Chem.* **276**, 16328–16334.
Read, R. J. (1986). *Acta Cryst.* A**42**, 140–149.
Woodcock, J., Moazed, D., Cannon, M., Davies, J. & Noller, H. F. (1991). *EMBO J.* **10**, 3099–3103.
Wright, G. D. & Ladak, P. (1997). *Antimicrob. Agents Chemother.* **41**, 956–960.
Wybenga-Groot, L. E., Draker, K., Wright, G. D. & Berghuis, A. M. (1999). *Structure Fold. Des.* **7**, 497–507.